Sea surface temperature control on the aerosol-induced brightness of marine clouds over the North Atlantic Ocean

Xiaoli Zhou[1,2], Jianhao Zhang[1,2,3], Graham Feingold[1,2]

[1]Chemical Sciences Laboratory, NOAA, Boulder, Colorado, USA
[2]Cooperative Institute for Research in Environmental Sciences (CIRES), University of Colorado, Boulder, Colorado, USA
[3]National Research Council, National Academies of Sciences, Engineering, Medicine (NASEM), Washington DC, USA

Key Points:

- SST has a strong influence on the relative occurrence of aerosol-induced brightness of clouds over the North Atlantic Ocean
- Aerosol perturbation is locally confined and has less influence on the brightness of clouds compared to SST
- In a warmer climate, we expect aerosol-induced cloud darkening caused by increased entrainment drying unless the clouds are very thin

Corresponding author: Xiaoli Zhou, `xiaoli.zhou@noaa.gov`

Abstract

Marine low clouds are one of the greatest sources of uncertainty for climate projection. We present an observed climatology of cloud albedo susceptibility to cloud droplet number concentration perturbations (S_0) with changing sea surface temperature (SST) and estimated inversion strength for single-layer warm clouds over the North Atlantic Ocean, using eight years of satellite and reanalysis data. The keyfindings are that SST has a dominant control on S_0 in the presence of co-varying synoptic conditions and aerosol perturbations. Regions conducive to aerosol-induced darkening (brightening) clouds occur with high (low) local SST. Higher SST significantly hastens cloud-top evaporation with increasing aerosol loading, by accelerating entrainment and facilitating entrainment drying. In a global-warming-like scenario, cloud darkening is expected, mainly as a result of increased entrainment drying via Clausius-Clapeyron scaling. Our results imply a more (less) positive low-cloud liquid water path feedback in a warmer climate with increasing (decreasing) aerosol loading.

Plain Language Summary

Low clouds over the ocean are a poorly quantified component of the climate system. Here we use eight years of space-based measurements and atmospheric reanalysis data to quantify how the reflectivity of single-layer low clouds over the North Atlantic Ocean responds to cloud droplet number concentration perturbations, under simultaneous sea surface temperature and temperature inversion strength changes. We find that under higher sea surface temperature, drop number increases tend to reduce cloud reflectivity by accelerating evaporation of cloud water. These results suggest that under global warming, low clouds might reflect less energy to space in response to an increase in aerosol loading, which will strengthen greenhouse gas forcing. If in the future, particle emissions are reduced, then we anticipate some offsetting of greenhouse gas forcing by brighter clouds.

1 Introduction

Marine low clouds are ubiquitous over the subtropical and midlatitude oceans (Wood, 2012) and strongly regulate the Earth's radiation budget by reflecting solar radiation back to space (Klein & Hartmann, 1993; Stephens et al., 2012). How low clouds will respond to changes in regional and global climate change is still uncertain and constitutes a major uncertainty in predictions of climate sensitivity (Bony & Dufresne, 2005; Dufresne & Bony, 2008; Vial et al., 2013; Zelinka et al., 2020). A primary source of spread in general circulation model (GCM)-derived climate sensitivity is the entrainment process at cloud top (Caldwell et al., 2013; M. Zhang et al., 2013; Rieck et al., 2012; Bretherton et al., 2013; Bretherton & Blossey, 2014; Sherwood et al., 2014), which responds to the change in sea surface temperature (SST) and lower tropospheric stability (LTS; Qu et al., 2015; Ceppi & Nowack, 2021) under global warming. Recent observational constraint studies predict positive shortwave cloud feedbacks across the subtropics and midlatitudes (Myers & Norris, 2016; Myers et al., 2021; Ceppi & Nowack, 2021) due to a decrease in boundary layer cloud cover (Qu et al., 2015; Zhai et al., 2015; McCoy et al., 2017). This feature is corroborated by long-term trends in observed cloud cover (Norris et al., 2016).

The uncertainty in climate projection is exacerbated by the effect of anthropogenic atmospheric aerosols on global cloud radiative forcing through changes in cloud amount and brightness. One of the strongest aerosol indirect effects occurs via changes to cloud condensate (Albrecht, 1989), which is typically quantified via observations of the response of cloud liquid water path (CWP) to aerosol-induced perturbations (Chen et al., 2014). Chen et al. (2014) identify LTS and free tropospheric relative humidity (RH_{ft}) as important controls on the aerosol-induced cloud water adjustment and the strength of aerosol-cloud radiative forcing. They find that for a drier free troposphere and lower tropospheric stability, CWP decreases with increasing aerosol due to a strengthened entrainment rate and evaporation efficiency induced by smaller cloud droplets (i.e., greater droplet surface areas) and weaker sedimentation (evaporation-entrainment feedbacks; Wang et al., 2003; Ackerman et al., 2004), which could counter the Twomey effect (enhanced albedo from more but smaller droplets; Twomey, 1974) and lead to lower cloud albedo (A_c). Existing studies only partially address the difficult problem of causality. How the governing meteorological factors co-vary with each other and with aerosol perturbations, and how cloud water adjustment is related to greenhouse gas-warming-induced changes is barely discussed in the existing literature. The latter is currently neglected in the current method of diagnosing aerosol forcing in GCMs (Mülmenstädt & Feingold, 2018).

In this study, we present an observed climatology of A_c susceptibility to cloud droplet number concentration (N_d) perturbations with changing SST and estimated inversion strength (EIS; Wood & Bretherton, 2006)–two key meteorological cloud-controlling factors (Qu et al., 2015; Klein et al., 2017; Ceppi & Nowack, 2021), for single-layer warm (liquid-phase) clouds in the planetary boundary layer (PBL) over the North Atlantic Ocean, where there is a wide range in SST. We show that by modulating inversion stability and cloud-top humidity, SST has a strong influence on the relative occurrence of aerosol-induced cloud brightening on daily and inter-annual timescales. Our results suggest a more frequent occurrence of less reflective clouds (darkening) with increased aerosol loading under global warming. The results presented here might be linked to a more (less) positive low-cloud liquid water path feedback in a warmer climate with increasing (decreasing) aerosol loading.

2 Data Set Description

We use 8 years (2003-2011) of the National Aeronautics and Space Administration (NASA) A-Train satellite measurements and European Center for Medium range Weather Forecast (ECMWF)'s fifth generation atmospheric reanalysis (ERA5) over the North Atlantic Ocean (25^{o}N 55^{o}N; 50^{o}W 15^{o}W) for single-layer liquid phase clouds.

Cloud properties including cloud water path (CWP), cloud optical depth, effective radius of cloud droplets, cloud top height and temperature, cloud phase, and cloud layers are sourced from Collection 6.1 daytime ($\sim$ 13:30 pm local time) marine cloud retrievals at 1 km (nadir) resolution from MODerate-resolution Imaging Spectroadiometer (MODIS) on the Aqua satellite. All cloud properties are averaged over time and space within the footprint ($\sim$ 20 km) of the Clouds and Earth's Radiant Energy System (CERES). The CERES footprint-level cloud property products are included in the CERES Single Scanner Footprint (SSF) level 2 Edition 4A dataset.

Rain rate data is sourced from the Advanced Microwave Scanning Radiometer for Earth Observing System (AMSR-E; Wentz & Meissner, 2004), provided on a non-uniform grid within a 1445 km-wide swath with a pixel resolution of $\sim$ 10 km at the center of the track.

We derive N_d using visible cloud optical depth and effective radius of cloud droplets measured in the 3.7 µm channel following Grosvenor et al. (2018). To ensure robust N_d retrievals, we confine our analysis to full coverage (100% cloud cover within the CERES footprint), single-layer liquid phase clouds with cloud top height no greater than 2 km and cloud top temperature no less than 273 K. Clouds with optical depth less than 1 are considered too thin for a reliable N_d retrieval and are therefore removed from the analysis. Only N_d retrievals less than 600 cm^{-3} are used in this study.

Since this study focuses on full cloud coverage within the CERES footprint, we estimate A_c from the all-sky albedo computed as the ratio of upward to incoming solar irradiance at the top-of-atmosphere (TOA) measured by CERES. The computed A_c is normalized by its value at 0^{o} solar zenith angle (SZA). We restrict the SZA to less than 65^{o} for reliable albedo calculation.

The environmental conditions are sourced from ERA5 reanalysis with a resolution of 0.25^{o}. The inversion strength is estimated from EIS derived from the ERA5 temperature at the surface and at 700 hPa following Wood and Bretherton (2006). As a refinement of LTS, EIS is a better predictor of inversion strength over the midlatitude oceans, where the free troposphere is cooler than in the tropics. Since we focus on boundary layer clouds below 2 km, we consider the absolute (relative) humidity at 800 hPa from ERA5 as a proxy for the free tropospheric absolute (relative) humidity. We compute the 900 hPa aerosol number concentration (N_a) from ERA5 aerosol mass at 900 hPa following Boucher and Lohmann (1995). Using vertical temperature and humidity profiles from ERA5, we identify the inversion as the level around the maximum increase in temperature with a height that occurs below 2 km, and has an increase in temperature and a decrease in absolute humidity (Rémillard et al., 2012; Zhou et al., 2015). The sea surface temperature (SST) is sourced from ERA5.

To merge the CERES footprint level data, AMSR-E rain rate data, and ERA5 reanalysis in the same study, we re-grid all data onto the CERES resolution (0.2$^{\text{o}}$) using nearest-neighbor interpolation. We further divide the data into 2$^{\text{o}}\times$2$^{\text{o}}$ latitude-longitude scenes. In each scene where scene-level cloud fraction (f_c) is greater than 0.25, the natural log of A_c from cloudy pixels is regressed onto the natural log of N_d. The resulting linear regression coefficient is an estimate of $S_0 = dln(A_c)/dln(N_d)$, defined as the A_c susceptibility to N_d perturbations. The logarithmic form reduces the sensitivity of S_0 to the measurement accuracy of A_c and N_d. The 2$^{\text{o}}$ $\times$ 2$^{\text{o}}$ scene is big enough to include variability in cloud properties, and small enough to guarantee nearly homogeneous meteorological conditions within the scene, such that the regression coefficients computed from the satellite swaths can be reasonably considered as the sensitivity of A_c to an N_d perturbation for a certain meteorological state. All other variables including SST, EIS, CWP, cloud top height (a proxy for inversion height), rain rate, absolute humidity at 800 hPa (q_{800}) and at the inversion (q_{inv}), relative humidity at 800 hPa (RH_{800}) and at 1000 hPa (RH_{1000}), N_d, and N_a at 900 hPa are averaged in cloudy pixels for each scene. In total 6562 samples are included. It is possible that the large-scale forcing might not equilibrate with cloud properties, which is also common in the mean state of the climate. The corresponding cloud radiative susceptibility at TOA is estimated from cloudy pixels in each scene following $F_c = dA_c/dln(N_d)SW_{TOAdn}$ [W m$^{-2}ln(N_d)^{-1}$], where SW_{TOAdn} is downward shortwave radiation at TOA.

3 Results

Bin-averaged S_0 with respect to EIS and RH_{800} in our study (Fig. 1a) resembles closely Fig. 1 in Chen et al. (2014), supporting the finding that darkening clouds (defined as negative S_0) favor dry overlying air and a relatively unstable boundary layer. Over 64% of the samples are of EIS between 4 K and 12 K, with RH_{800} varying widely from 0 to 80% (Fig. 1a). The frequency-weighted average S_0 over the North Atlantic is -0.03, corresponding to F_c of -12 $Wm^{-2}ln(N_d)^{-1}$. Comparing Fig. 1b with Fig. 1a shows that bin-averaged SST over the North Atlantic varies with an almost opposite trend to S_0 with respect to EIS and RH_{800}, suggesting that SST has a strong control on the aerosol-induced brightness of marine clouds over the North Atlantic Ocean by modulating lower tropospheric stability and free tropospheric relative humidity (RH). Regions prone to an aerosol-related darkening of clouds occur at high local SST.

The control of SST on S_0 is seen clearly in Fig. 2a where S_0 is now plotted in the EIS – SST space. The bin-averaged S_0 is predominantly negative (darkening) for SST>290 K, regardless of EIS. For SST < 290 K, S_0 is mostly positive or near zero. EIS appears to be a good indicator of warm precipitation (Fig. 2b), such that relatively high EIS (EIS > 7 K) is associated with none or very lightly precipitating clouds (rain rate < 0.3 mm day^{-1}) and precipitation tends to increase with decreasing EIS. In this sense, the EIS – SST space can be broadly divided into four Quadrants — Quadrant I (upper right): nonprecipitating darkening clouds, Quadrant II (upper left): nonprecipitating brightening clouds, Quadrant III (lower left): precipitating brightening clouds, and Quadrant IV (lower right): precipitating darkening clouds. It can be inferred from Figs. 2a and 2b that the aerosol-induced brightening of marine clouds is not directly related to the occurrence of precipitation. We will elaborate below on why darkening clouds tend to occur in Quadrants I & IV where SST is relatively high.

Ideally, EIS would depend solely on SST if the overlying temperature in the free troposphere were to remain unchanged (e.g., unchanged remote tropical SST and fixed season). In this scenario, the evolution of the PBL and cloud properties along the prevailing winds follows the diagonal from the top left to the bottom right corner in the EIS – SST space, along which EIS is negatively correlated with SST. All else equal, higher local SST deepens the boundary layer by reducing EIS along the diagonal (Fig. 2c). The deepening boundary layer is associated with reduced cloud top absolute humidity (Fig. 2d) since free tropospheric absolute humidity tends to decrease with height by nature. Our results show that a $\sim$1 km deeper boundary layer corresponds to a $\sim$2 g kg^{-1} reduction in the cloud top absolute humidity. The relatively unstable lower troposphere and drier overlying air serve to accelerate cloud-top entrainment and facilitate cloud top evaporation and therefore favor cloud darkening.

Even with the strong difference in cloud top heights, the bin-averaged CWPs along the diagonal are comparable (Fig. 2e), likely due to the counteracting effects of a deeper inversion layer and higher cloud base at lower EIS. This suggests that the radiative cooling driving cloud-top turbulence is not the dominant control on the entrainment along the diagonal. We also examine the influence of precipitation scavenging of cloud water on cloud darkening in Quadrant IV and find that precipitation plays a negligible role (Text S1; Figs. S1 and S2).

If the free tropospheric temperature changes at a similar or faster rate than the SST (e.g., SST changes locally and remotely (Wood & Bretherton, 2006; Qu et al., 2014, 2015) or season changes), EIS would change only marginally or positively with SST. This corresponds to a horizontal or diagonal from bottom left to top right corner in the EIS-SST space in Fig. 2.

In this aforementioned scenario, assuming the same absolute humidity, higher SST corresponds to warmer free tropospheric air that can dramatically decrease free tropospheric RH as per the Clausius-Clapeyron scaling (Fig. S3), and thereby enhance entrainment drying of the boundary layer. The drier boundary layer triggers an increase in latent heat fluxes (LHF), which weakens the RH reduction in the boundary layer (Fig. S3). This leads to an increased humidity difference between dry free tropospheric air and boundary layer air with increasing SST (Fig. 2f). Analytical calculation shows that with a fixed EIS of 10 K, increasing local SST from 285 K to 295 K reduces RH_{800} by $\sim$50% for a given q_{800}. The stronger humidity difference at the inversion (ΔRH) is known to decrease low cloud fraction and amount through cloud top entrainment (Lock, 2009; Bretherton et al., 2013; Qu et al., 2015). Here we show that the ΔRH also facilities negative S_0 and might further strengthen the positive cloud liquid water path feedback with increasing aerosol levels. Regions of high SST and EIS (Quadrant I) are associated with the warmest and thus driest free tropospheric air and hence experience the strongest ΔRH at cloud top (Fig. 2f).

With the increase in ΔRH (and also LHF) in this scenario, CWP reduces correspondingly (Fig. 2e). This is attributable to an increase in the LHF-induced in-cloud buoyancy fluxes, such that a small CWP is enough to generate comparable cloud top turbulence to sustain the boundary layer (Bretherton et al., 2013). These comparable levels of turbulence translate to similar entrainment rates; therefore it is the enhanced entrainment drying, rather than entrainment rate, that facilitates the cloud darkening. Note that when CWP is very low ($<50 \sim 60$ g m^{-2}), negative cloud adjustment is more than overcome by the enhanced Twomey effect and therefore S_0 becomes positive (J. Zhang et al., 2021).

The background aerosol concentrations are in general quite homogeneous over the North Atlantic region, except in Quadrants I and III where the bin-averaged N_a are slightly higher

(Fig. 2g). This is due to a slightly higher frequency of occurrence of large N_a ($N_a > 200$ cm^{-3}) in Quadrants I and III (∼30 %) compared to the other Quadrants (∼20 %). The higher N_a emanates from the European Continent and Greenland via favorable synoptic patterns (Fig. S4). As a result, the bin-averaged N_d is slightly higher in Quadrants I and III (Fig. 2h).

N_d is one of the important cloud properties (the other is CWP) that can directly modify S_0, by determining cloud droplet sedimentation velocity, precipitation, and the Twomey effect. We do find a negative correlation between S_0 and N_d over the North Atlantic. Clouds with low N_d (< 30 cm^{-3}) tend to be associated with positive S_0 (Fig. S5), which we attribute to be mainly driven by reduced evaporation-entrainment feedbacks and enhanced precipitation suppression when rain is present. Further analysis shows that the decreasing trend of S_0 with SST is not sensitive to the natural N_d variation (Figs. S6-S8). This reflects the governing of S_0 by large-scale environmental conditions in the presence of local aerosol perturbations. The frequency-weighted averaged S_0 (F_c), however, is sensitive to N_d: S_0 (F_c) is 0.05 (12 W m^{-2} $ln(N_d)^{-1}$), -0.08 (-24 W m^{-2} $ln(N_d)^{-1}$), and -0.04 (-19 W m^{-2} $ln(N_d)^{-1}$) for $N_d < 30$ cm^{-3}, $30 \leq N_d < 60$ cm^{-3}, $N_d \geq 60$ cm^{-3} respectively.

4 Seasonal and inter-annual variability

In this section, we investigate how seasonal variation influences the control of SST on S_0. Due to the strong seasonal variability in the Hadley circulation, the free tropospheric absolute humidity shows a strong seasonal variation across all SSTs (Fig. 3a). The stronger zonally averaged Hadley circulation (i.e., lower temperature at greater height) and weaker solar insolation (colder air) in winter result in drier free tropospheric air in the Northern Hemisphere subtropics as per the Clausius-Clapeyron relation. As a result, the q_{800} in June, July, and August (JJA) is ∼5 g kg^{-1}, about three times as much as that in December, January, and February (DJF) (∼1.5 g kg^{-1}) (Fig. 3a).

Warmer free tropospheric air in JJA due to stronger solar radiation reduces the difference in free tropospheric RH between the seasons, although JJA is still significantly moister (Fig. 3b). Warmer free tropospheric air in JJA also leads to a stronger EIS across all SST compared to DJF (Fig. 3c), both of which inhibit cloud top entrainment and evaporation, lowering the boundary layer height (Fig. 3d) and hampering cloud darkening.

N_d over the North Atlantic also appears to be seasonally dependent, with N_d increasing by nearly 25 % in JJA, and amplifies with SST (Fig. 3e). The increase in N_d with SST in JJA relative to DJF counteracts their difference in environmental conditions by enhancing evaporation-entrainment feedbacks. The counteracting effects of microphysical (N_d) and environmental (q_{800}, EIS) controls result in a comparable trend of S_0 with respect to SST in winter and in summer. There is a slightly more frequent occurrence of darkening clouds in winter as indicated by the close spacing between dots and shift of the blue shading towards negative S_0, suggesting a slightly more dominant influence of environmental control over microphysical control on S_0.

The control of SST on S_0 is shown to be much more significant than the control of N_d at the inter-annual time scale. S_0 shows an apparent anti-correlation with SST in both seasons (with correlation coefficient R ∼ -0.4), especially in DJF when the year-to-year SST spans a greater range (Fig. 4).

5 Discussion

The wide spatial variability in SST over the North Atlantic Ocean has allowed us to examine the response of S_0 to varying SST environments that are less contaminated by the seasonal co-variability between meteorological conditions. In regions with more homogeneous SST (e.g., the North Eastern Pacific Ocean (NEP); J. Zhang et al., 2021), the seasonal co-variation of SST with free tropospheric absolute humidity is remarkable, in a way that high (low) SST correlates with more (less) humid overlying air in summer (winter) when solar radiation is stronger (weaker) and the Hadley circulation is weaker (stronger). The humid free tropospheric air at high SST prevents efficient cloud top evaporation and offsets to a large extent the response of S_0 to changing SST. This is likely the reason why the controlling role of SST is not reflected in the NEP (J. Zhang et al., 2021) and other stratocumulus–dominant regions (Qu et al., 2015).

We note that this study only looks at full coverage clouds at the CIRES pixel level ($\sim$20 km), which eliminates most of the low coverage open cell regime where it is more common to find enhanced precipitation. As a result, the clouds in this study are mostly precipitation free or lightly precipitating (92 % of samples have rain rate < 1 mm day^{-1}), such that aerosol-related increases in cloud water accompanying suppressed precipitation are less than cloud water losses associated with increased cloud-top entrainment. Clouds with more enhanced precipitation (lower N_d) are found to brighten with an increase in aerosol loading (Christensen & Stephens, 2012; J. Zhang et al., 2021).

The domain-averaged S_0 (-0.03) and F_c (-12 W m^{-2} $ln(N_d)^{-1}$) are calculated from cloudy pixels in each scene. Considering the mean cloud fraction at each scene ($\sim$0.5), the radiative susceptibility due to the combined cloud water adjustment and Twomey effect over the North Atlantic is -6.9 W m$^{-2}ln(N_d)^{-1}$. This number might be less negative if scenes with cloud fraction less than 0.25 are included. The adjustment of cloud fraction to N_d might also affect the total radiative aerosol effect, but we are not able to assess this information using the current dataset.

The analysis shown in this study includes samples with all possible correlation coefficients between cloud albedo and N_d. A stricter refinement (e.g., $|R| > 0.5$) leads to more negative S_0 (-0.06) and F_c (-22.7 W m$^{-2}ln(N_d)^{-1}$), and a stronger dependence of S_0 on SST (Fig. S9). With the current dataset, we cannot assess the diurnal variability of S_0, nor can we assess how S_0 responds to increased CO_2, whose direct radiative effect (downwelling longwave radiation) is thought to reduce the cloud-top radiative cooling and therefore thin the clouds (Bretherton et al., 2013). Further observational or numerical studies are encouraged in this regard.

6 Conclusions

This study presents an observed climatology of the marine cloud albedo susceptibility to perturbations in cloud droplet number concentration (S_0) and its relation to sea surface temperature (SST) and related environmental conditions, using eight years of A-Train satellite measurements and reanalysis data. We find a strong control of SST on S_0; higher SST facilitates a greater entrainment rate (by increasing boundary layer instability) and entrainment drying (by deepening the cloud layer and creating a stronger humidity gradient at the inversion), both of which hasten evaporation at cloud top. With increasing aerosol burden, the evaporation is further enhanced via evaporation-entrainment feedbacks. As a result, higher SST is associated with a higher frequency of less reflective clouds and thus more negative S_0 with increasing aerosol loading. The exception is when clouds are very thin with CWP $< 50 \sim 60$ g m^{-2}. We find that the aerosol perturbation is more locally confined and therefore more than offset by the perturbations of SST-induced environmental conditions and their control on S_0. Seasonal and inter-annual variability in SST and S_0 support our findings. Synoptic disturbances could affect the frequency of occurrence of clouds with different degrees of precipitation and brightness, but they are less important in determining cloud albedo susceptibility compared to the large-scale environmental conditions (e.g., seasonal variability; local SST) (Fig. S4).

Projecting these results to a global-warming-like scenario where free tropospheric temperature changes at a similar or faster rate than SST, and where the moisture contrast is enhanced (because surface humidity generally increases at a higher rate than free tropospheric humidity according to the Clausius-Clapeyron relation (Qu et al., 2015; Bretherton et al., 2013), and because the relative humidity of mixed air parcels at the inversion tends to reduce at a higher temperature (Rieck et al., 2012)), cloud darkening would be mainly caused by increased entrainment drying. Our results provide insights into a future where if (1) a warmer climate produces higher natural aerosol emissions, the aerosol forcing associated with aerosol-cloud interactions will increase, leading to a more positive cloud liquid water path feedback; or conversely if (2) anthropogenic aerosol emissions are reduced, the aerosol forcing associated with aerosol-cloud interactions will decrease, mitigating the positive cloud liquid water path feedback.

Acknowledgments

We gratefully acknowledge funding from the U.S. Department of Energy, Office of Science, Atmospheric System Research Program Interagency Award 89243020SSC000055 and from an Earth's Radiation Budget grant, NOAA CPO Climate CI 03-01-07-001. JZ was supported by a National Research Council Research Associateship award at the National Oceanic and Atmospheric Administration (NOAA). We acknowledge the Clouds and Earth's Radiant Energy System (CERES)'s Single Scanner Footprint (SST) level 2 Edition 4A dataset at https://ceres-tool.larc.nasa.gov/ord-tool/products?CERESProducts=SSFlevel2_Ed4); the European Center for Medium range Weather Forecast (ECMWF)'s fifth generation atmospheric reanalysis (ERA5) data at https://cds.climate.copernicus.eu/cdsapp#!/dataset/reanalysis-era5-pressure-levels?tab=overview; the Advanced Microwave Scanning Radiometer for Earth Observing System rain rate data at https://nsidc.org/data/AE_Rain.

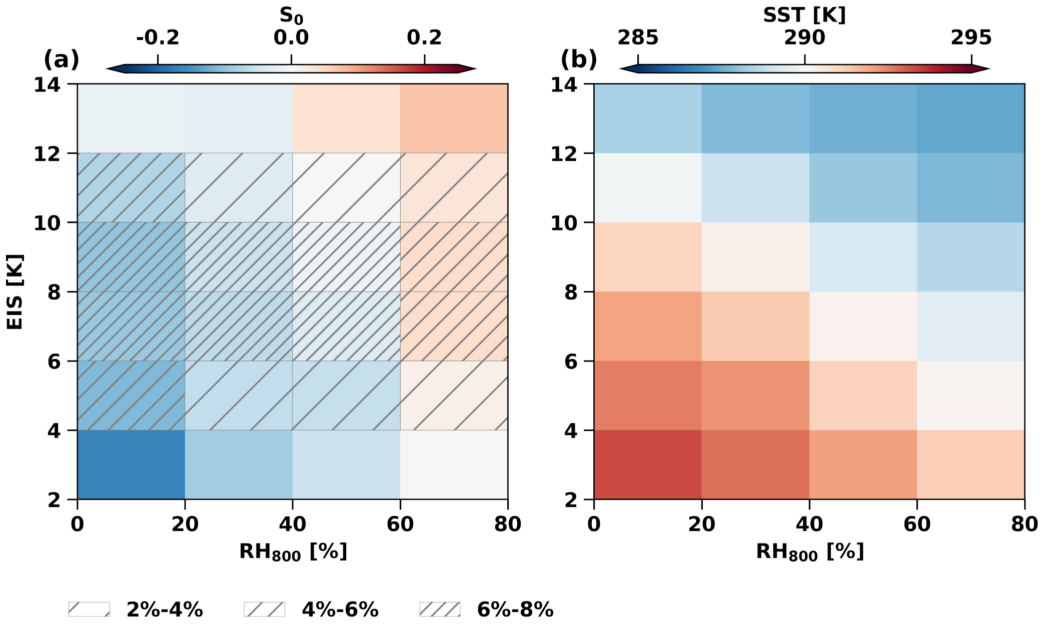

Figure 1. (a) The mean values of susceptibility of cloud albedo to the cloud droplet number concentration (S_0) within bins of estimated inversion strength (EIS) and relative humidity at 800 hPa (RH_{800}). The bin width is 2K ΔEIS in the vertical and 20% ΔRH_{800} in the horizontal. At least 20 samples are required in each bin. Hatches in (a) indicate the frequency of occurrence in each bin. Bins with no hatching have a frequency of occurrence below 2%. (b) Same as (a) but for sea surface temperature (SST).

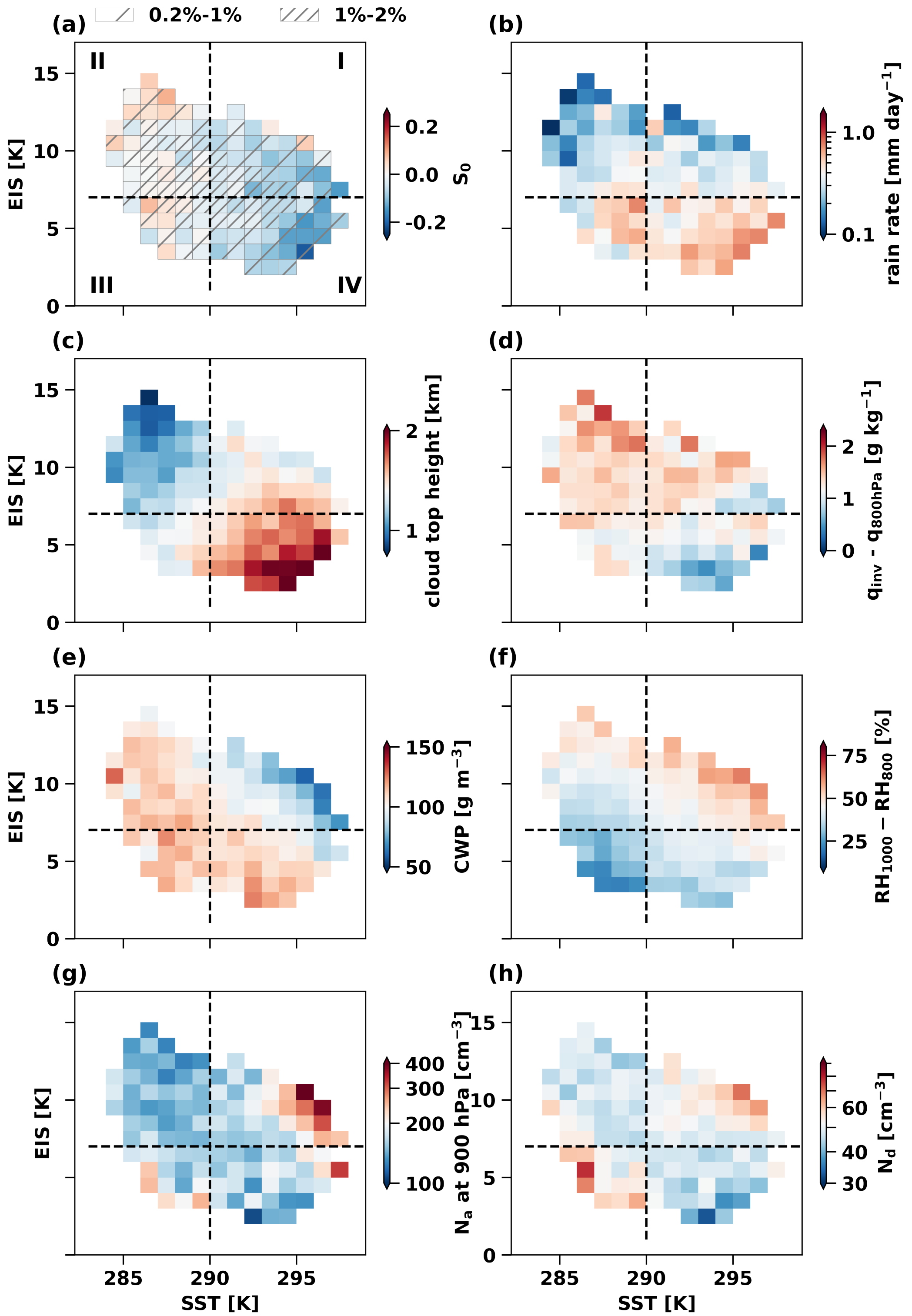

Figure 2. The mean values of (a) susceptibility of cloud albedo to cloud droplet number concentration(S_0), (b) rain rate, (c) cloud top height, (d) absolute humidity difference between inversion top (q_{inv}) and 800 hPa (q_{800}), (e) cloud water path (CWP), (f) relative humidity difference between 1000 hPa (RH_{1000}) and 800 hPa (RH_{800}), (g) aerosol number concentration at 900 hPa (N_a), and (h) cloud droplet number concentration (N_d) within bins of estimated inversion strength and sea surface temperature. The bin width is 1K ΔEIS in the vertical and 1K ΔSST in the horizontal. At least 20 samples are required in each bin. Black dashes indicate SST = 290 K and EIS = 7 K isolines. The Roman numerals I, II, III, and IV in (a) indicate quadrants. Hatches in (a) indicate the frequency of occurrence in each bin. The bins with no hatching have a frequency of occurrence below 0.2%.

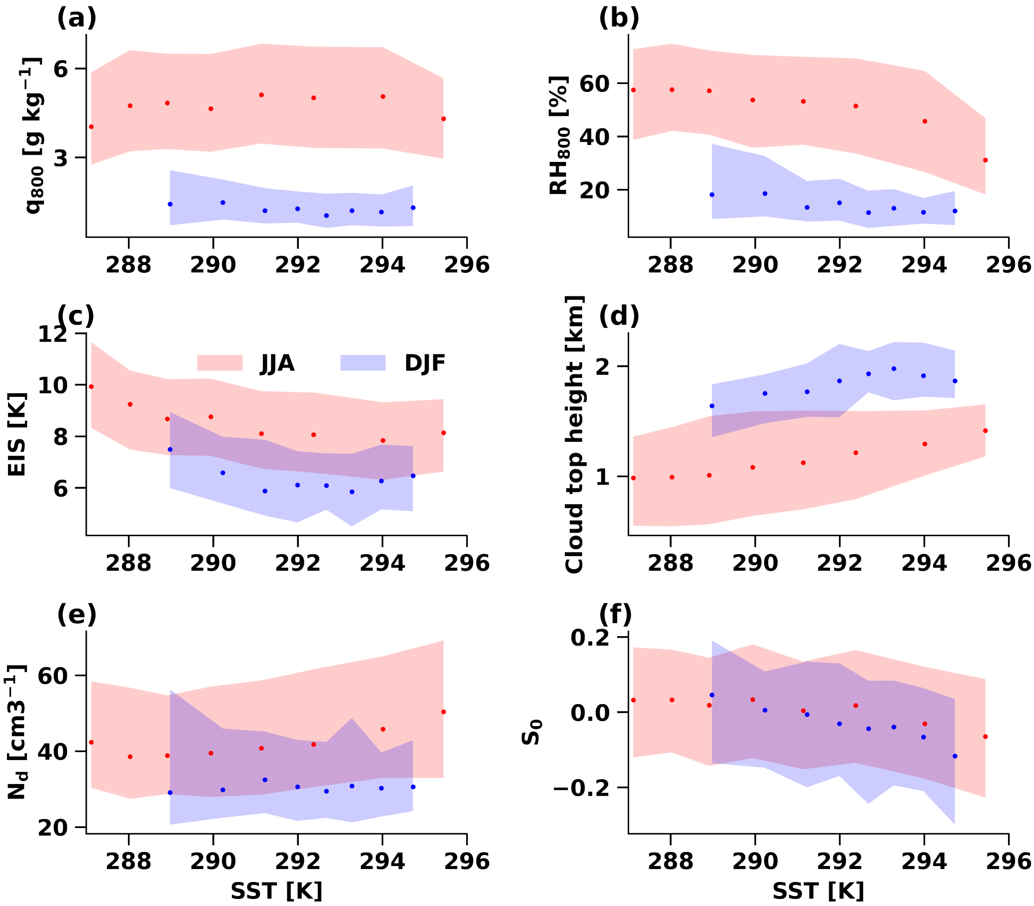

Figure 3. Quartiles of (a) absolute humidity at 800 hPa (q_{800}), (b) relative humidity at 800 hPa (RH_{800}), (c) estimated inversion strength (EIS), (d) cloud top height, (e) cloud droplet number concentration (N_d), and (f) susceptibility of cloud albedo to cloud droplet number concentration (S_0), within sea surface temperature (SST) bins for June, July, and August (JJA, red) and December, January, and February (DJF, blue). Dots indicate median values within SST bins (10 %).

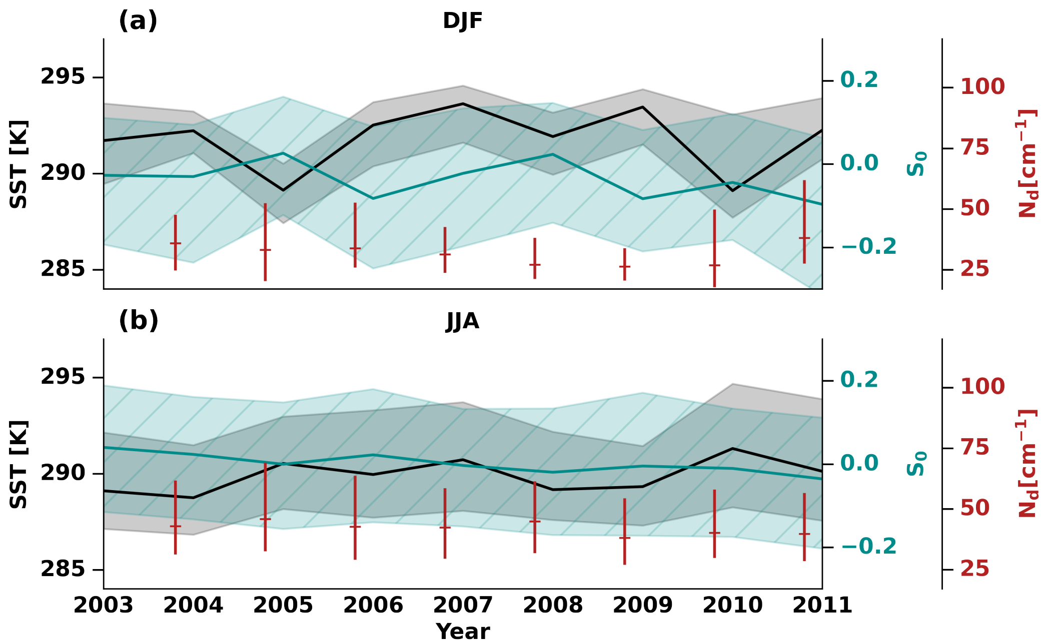

Figure 4. The annual median (solid line) and quartile (shading) of sea surface temperature (SST, black) and susceptibility of cloud albedo to cloud droplet number concentration (S_0, dark blue) for (a) December, January, and February (DJF) and (b) June, July, and August (JJA) from 2003 to 2011. The annual medians and interquartile ranges of cloud droplet number concentration (N_d) are indicated by red horizontal and vertical line markers.

References

Ackerman, A. S., Kirkpatrick, M. P., Stevens, D. E., & Toon, O. B. (2004). The impact of humidity above stratiform clouds on indirect aerosol climate forcing. *Nature*, *432*(7020), 1014–1017.

Albrecht, B. A. (1989). Aerosols, cloud microphysics, and fractional cloudiness. *Science*, *245*(4923), 1227–1230.

Bony, S., & Dufresne, J.-L. (2005). Marine boundary layer clouds at the heart of tropical cloud feedback uncertainties in climate models. *Geophysical Research Letters*, *32*(20).

Boucher, O., & Lohmann, U. (1995). The sulfate-ccn-cloud albedo effect. *Tellus B: Chemical and Physical Meteorology*, *47*(3), 281–300.

Bretherton, C. S., & Blossey, P. N. (2014). Low cloud reduction in a greenhouse-warmed climate: Results from lagrangian les of a subtropical marine cloudiness transition. *Journal of Advances in Modeling Earth Systems*, *6*(1), 91–114.

Bretherton, C. S., Blossey, P. N., & Jones, C. R. (2013). Mechanisms of marine low cloud sensitivity to idealized climate perturbations: A single-les exploration extending the cgils cases. *Journal of Advances in Modeling Earth Systems*, *5*(2), 316–337.

Caldwell, P. M., Zhang, Y., & Klein, S. A. (2013). Cmip3 subtropical stratocumulus cloud feedback interpreted through a mixed-layer model. *Journal of Climate*, *26*(5), 1607–1625.

Ceppi, P., & Nowack, P. (2021). Observational evidence that cloud feedback amplifies global warming. *Proceedings of the National Academy of Sciences*, *118*(30).

Chen, Y.-C., Christensen, M. W., Stephens, G. L., & Seinfeld, J. H. (2014). Satellite-based estimate of global aerosol–cloud radiative forcing by marine warm clouds. *Nature Geoscience*, *7*(9), 643–646.

Christensen, M. W., & Stephens, G. L. (2012). Microphysical and macrophysical responses of marine stratocumulus polluted by underlying ships: 2. impacts of haze on precipitating clouds. *Journal of Geophysical Research: Atmospheres*, *117*(D11).

Dufresne, J.-L., & Bony, S. (2008). An assessment of the primary sources of spread of global warming estimates from coupled atmosphere–ocean models. *Journal of Climate*, *21*(19), 5135–5144.

Grosvenor, D. P., Sourdeval, O., Zuidema, P., Ackerman, A., Alexandrov, M. D., Bennartz, R., et al. (2018). Remote sensing of droplet number concentration in warm clouds: A review of the current state of knowledge and perspectives. *Reviews of Geophysics*, *56*(2), 409–453.

Klein, S. A., Hall, A., Norris, J. R., & Pincus, R. (2017). Low-cloud feedbacks from cloud-controlling factors: A review. *Shallow clouds, water vapor, circulation, and climate sensitivity*, 135–157.

Klein, S. A., & Hartmann, D. L. (1993). The seasonal cycle of low stratiform clouds. *Journal of Climate*, *6*(8), 1587–1606.

Lock, A. (2009). Factors influencing cloud area at the capping inversion for shallow cumulus clouds. *Quarterly Journal of the Royal Meteorological Society: A journal of the atmospheric sciences, applied meteorology and physical oceanography*, *135*(641), 941–952.

McCoy, D. T., Eastman, R., Hartmann, D. L., & Wood, R. (2017). The change in low cloud cover in a warmed climate inferred from airs, modis, and era-interim. *Journal of Climate*, *30*(10), 3609–3620.

Mülmenstädt, J., & Feingold, G. (2018). The radiative forcing of aerosol–cloud interactions in liquid clouds: Wrestling and embracing uncertainty. *Current Climate Change Reports*, *4*(1), 23–40.

Myers, T. A., & Norris, J. R. (2016). Reducing the uncertainty in subtropical cloud feedback. *Geophysical Research Letters*, *43*(5), 2144–2148.

Myers, T. A., Scott, R. C., Zelinka, M. D., Klein, S. A., Norris, J. R., & Caldwell, P. M. (2021). Observational constraints on low cloud feedback reduce uncertainty of climate sensitivity. *Nature Climate Change*, *11*(6), 501–507.

Norris, J. R., Allen, R. J., Evan, A. T., Zelinka, M. D., O'Dell, C. W., & Klein, S. A. (2016). Evidence for climate change in the satellite cloud record. *Nature*, *536*(7614), 72–75.
Qu, X., Hall, A., Klein, S. A., & Caldwell, P. M. (2014). On the spread of changes in marine low cloud cover in climate model simulations of the 21st century. *Climate dynamics*, *42*(9-10), 2603–2626.
Qu, X., Hall, A., Klein, S. A., & Caldwell, P. M. (2015). The strength of the tropical inversion and its response to climate change in 18 cmip5 models. *Climate Dynamics*, *45*(1-2), 375–396.
Rémillard, J., Kollias, P., Luke, E., & Wood, R. (2012). Marine boundary layer cloud observations in the azores. *Journal of Climate*, *25*(21), 7381–7398.
Rieck, M., Nuijens, L., & Stevens, B. (2012). Marine boundary layer cloud feedbacks in a constant relative humidity atmosphere. *Journal of the Atmospheric Sciences*, *69*(8), 2538–2550.
Sherwood, S. C., Bony, S., & Dufresne, J.-L. (2014). Spread in model climate sensitivity traced to atmospheric convective mixing. *Nature*, *505*(7481), 37–42.
Stephens, G. L., Li, J., Wild, M., Clayson, C. A., Loeb, N., Kato, S., et al. (2012). An update on earth's energy balance in light of the latest global observations. *Nature Geoscience*, *5*(10), 691–696.
Twomey, S. (1974). Pollution and the planetary albedo. *Atmospheric Environment (1967)*, *8*(12), 1251–1256.
Vial, J., Dufresne, J.-L., & Bony, S. (2013). On the interpretation of inter-model spread in cmip5 climate sensitivity estimates. *Climate Dynamics*, *41*(11-12), 3339–3362.
Wang, S., Wang, Q., & Feingold, G. (2003). Turbulence, condensation, and liquid water transport in numerically simulated nonprecipitating stratocumulus clouds. *Journal of the atmospheric sciences*, *60*(2), 262–278.
Wentz, F., & Meissner, T. (2004). *Amsr-e/aqua l2b global swath ocean products derived from wentz algorithm, version 2. nasa national snow and ice data center distributed active archive center, accessed september 2015, doi: 10.5067* (Tech. Rep.). AMSR-E/AE_OCEAN. 002.
Wood, R. (2012). Stratocumulus clouds. *Monthly Weather Review*, *140*(8), 2373–2423.
Wood, R., & Bretherton, C. S. (2006). On the relationship between stratiform low cloud cover and lower-tropospheric stability. *Journal of climate*, *19*(24), 6425–6432.
Zelinka, M. D., Myers, T. A., McCoy, D. T., Po-Chedley, S., Caldwell, P. M., Ceppi, P., et al. (2020). Causes of higher climate sensitivity in cmip6 models. *Geophysical Research Letters*, *47*(1), e2019GL085782.
Zhai, C., Jiang, J. H., & Su, H. (2015). Long-term cloud change imprinted in seasonal cloud variation: More evidence of high climate sensitivity. *Geophysical Research Letters*, *42*(20), 8729–8737.
Zhang, J., Xiaoli, Z., & Graham, F. (2021). Albedo susceptibility regimes of marine low-level clouds and the covarying meteorological constraints over the northeast pacific stratocumulus region. *Atmospheric Chemistry and Physics*.
Zhang, M., Bretherton, C. S., Blossey, P. N., Austin, P. H., Bacmeister, J. T., Bony, S., et al. (2013). Cgils: Results from the first phase of an international project to understand the physical mechanisms of low cloud feedbacks in single column models. *Journal of Advances in Modeling Earth Systems*, *5*(4), 826–842.
Zhou, X., Kollias, P., & Lewis, E. R. (2015). Clouds, precipitation, and marine boundary layer structure during the magic field campaign. *Journal of Climate*, *28*(6), 2420–2442.